Research Article

Advances in Mechanical Engineering

Advances in Mechanical Engineering
2020, Vol. 12(9) 1–10

DOI: 10.1177/1687814020953941
journals.sagepub.com/home/ade
SAGE

Sheet thinning prediction method based on localized friction effect in deep-drawing

Pavaret Preedawiphat[1], Pramote Koowattanasuchat[1], Numpon Mahayotsanun[1] and Sasawat Mahabunphachai[2]

Abstract

The paper investigated the effect of localized friction on sheet thinning under lubricated conditions in the deep-drawing process. The Finite Element Analysis (FEA) was used to evaluate the sheet thinning of the AISI 304 sheet under six segmented blank-sheet interfaces. Different values of variable coefficient of friction (VCOF) in each segmented area were investigated, and the sheet thickness values at the considered areas were measured. The regression analysis models (Linear Regression, Response Surface Method, and Polynomial Regression) was used to determine the relationships between VCOF and sheet thinning. The results showed that the Linear Regression showed the best fit. The significant factor analysis was also carried out to determine how the localized friction affected the sheet thinning. The contributions of VCOF from at least two segmented areas affected the sheet thinning at any particular location. The obtained relationships of the VCOF and sheet thinning could be beneficial for the localized friction control for highly complex shapes.

Keywords

Deep-drawing, finite element analysis, formability, localized friction, regression analysis, sheet thinning

Date received: 1 March 2020; accepted: 30 July 2020

Handling Editor: James Baldwin

Introduction

Modern deep-drawn products are highly complex and require high formability parts. Several closed-loop control techniques (such as blank holder force control and multi-step forming with annealing) can be applied to increase the formability in the deep-drawing process.[1–4] In deep drawing, the influential factors were tool radius, friction coefficient, material flows, and blank holder force.[5] Spring back has been one of the major problems commonly found in sheet metal forming.[6] The material flow must be well controlled to prevent common defects (wrinkling and tearing), which can be observed in the forming limit curves (FLC).[7] There have also been many research investigations on how to test the sheet formability.[8–10]

Another critical factor that can affect the formability in the deep-drawing process is friction. Sniekers investigated frictional phenomena in deep-drawing and observed the subsurface deformations affecting the accuracy of the coefficient of friction (COF) calculation.[11] The effects of the blank holder force on friction in deep drawing were observed by Aleksandrović et al.[12] Hassan et al. performed the segmentation of blank holders under different friction conditions and found out that the local wrinkling problems could be

[1]Department of Mechanical Engineering, Faculty of Engineering, Khon Kaen University, Khon Kaen, Thailand
[2]National Metal and Materials Technology Center (MTEC), National Science and Technology Development Agency (NSTDA), Pathum Thani, Thailand

Corresponding author:
Numpon Mahayotsanun, Department of Mechanical Engineering, Faculty of Engineering, Khon Kaen University, Khon Kaen, 40002, Thailand.
Email: numpon@kku.ac.th

Table 1. Mechanical properties of materials considered in this study.

Parts	Materials	Tensile strength (N/mm^2)	Yield strength (N/mm^2)	Maximum elongation (%)	Hardness (HRC)
Die set	SKD11	–	–	–	58–62
Blank sheet	AISI 304	734	305	50	–
Lubricant	Active element	Appearance	Specific gravity (g/cm^3, 15°C)	Viscosity (mm^2/s, 40°C)	Copper corrosion test (100°C × 1 hr)
Forming oil	Chlorine (<20 wt%), Sulfur (<10 wt%), Fatty oil (<20 wt%)	Dark red transparent	1.0	135	2 (Inactive)

reduced by friction.[13] Olguner and Bozdana investigated friction effects on the punch load and thickness reduction in deep drawing.[14] Gil et al. used the pressure-dependent friction coefficient in predicting the springback of automotive parts and observed that the prediction was improved by considering the changes in friction under different pressures.[15] The influences of friction on the formability of steel sheets were examined by Tekaut.[16,17] According to the aforementioned studies, different areas in deep-drawing should be under different friction conditions or having a variable coefficient of friction (VCOF) to obtain the highest formability results.

Nevertheless, one of the main challenges in deep-drawing is to integrate VCOF in the process because the effect of variable friction conditions depends on many factors such as materials, geometries, and loading conditions. As a result, the effects of VCOF in deep-drawing to the formability should be understood. One of the commonly used tools is Finite Element Analysis (FEA) that can simulate and analyze the forming behaviors under different conditions.[18–23] In addition, the optimization methods have also been applied to predict forming behaviors in the deep-drawing process.[24–25] This paper integrated FEA and optimization methods to predict the effects of VCOF on formability in deep-drawing. Since the primary concern here was tearing, sheet thinning was used as an indicator for the formability. The predicted results would be helpful to prevent tearing, but the optimized VCOF values would also be essential for the closed-loop control in deep-drawing for highly complex shapes.

Methods and materials

Deep-drawing experiment

The sheet material investigated in this study was AISI 304. This type of material was the austenitic chromium-nickel stainless steel, providing excellent corrosion resistance.[26] The length of the blank was parallel to the rolling direction. The planar anisotropy of AISI 304, especially in the annealed condition, was neglected in this study. The tensile tests of the material were conducted to obtain the material flow curve (power-law), as shown in equation (1).

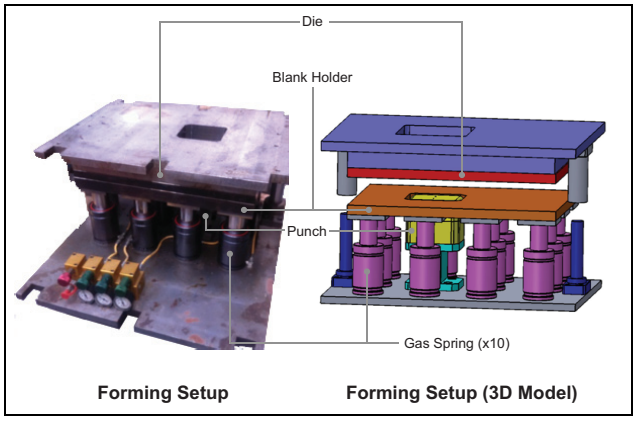

Figure 1. Deep-drawing setup.

$$\bar{\sigma} = 900 \cdot \bar{\varepsilon}^{0.365} \quad (1)$$

where $\bar{\sigma}$ is the flow stress, and $\bar{\varepsilon}$ is the true strain.

Each blank had a dimension of $337.5 \times 237.0 \times 0.4\ mm^3$ (Length × Width × Thickness). The punch dimensions were $112.06 \times 99.56 \times 45.0\ mm^3$ (Length × Width × Height). The die opening area was $113.02 \times 100.52\ mm^2$ (Length × Width), and the die radius was 1.0 mm. The blank holder plate was $440.0 \times 347.5 \times 30.0\ mm^3$ (Length × Width × Height). The material of the die set (punch, die, and blank holder) was SKD11. This type of material was the high-carbon and high-chromium alloy tool steel and had excellent wear resistance.[27] Figure 1 illustrates the deep-drawing setup, and Table 1 shows the mechanical properties of materials considered in this study.

The strip-drawing experiment was conducted to determine the coefficient of friction between the

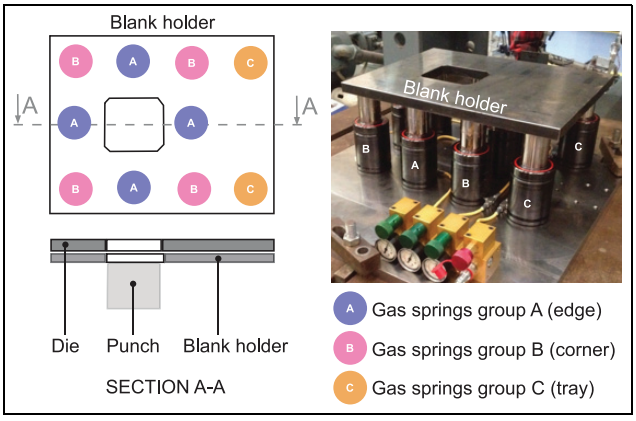

Figure 2. The blank holder setup.

tool-sheet interface under the considered lubricant.[28–29] The strip-drawing results showed that the COF was 0.125 for the entire tool-sheet interfaces. In this study, the deep drawing setup was located in the stamping press. The blank holder forces were set by using the nitrogen gas springs. Each nitrogen-gas spring could provide a maximum blank holder force (BHF) of 2.43 tons, and was set to various BHF levels by regulating the pressure inside the gas spring using a control valve, as shown in Figure 2. Note that the blank holder forces were set by changing pressure in each gas spring group. The punch speed was 10 mm/min, and the depth of the deep-drawn parts cup was 30 mm.

After each test, the percentage of thinning of sheet thickness after being deep-drawn was used as the formability indicator. The sheet thickness at three directions (0°, 45°, and 90°) was measured at 10 locations and repeated three times at the position by using a micrometer, as shown in Figure 3. The percentage of thinning was calculated by equation (2).

$$T\% = (T_{initial} - T_{final}) * 100/T_{initial} \quad (2)$$

where $T\%$ is the percentage of thinning, $T_{initial}$ is the initial blank sheet thickness (0.4 mm), and T_{final} is the final sheet thickness.

Numerical methods

Finite Element Analysis (FEA) was utilized to observe the forming behaviors under different friction conditions in deep-drawing. The deep-drawing process was modeled using commercial FE software MSC Patran 2015 and MSC Marc Mentat 2015. The MSC Patran 2015 was used for modeling rigid element surfaces of the die, punch, and gas spring cushion pins. MSC Marc Mentat 2015 was used as a model solver. The material flow curve of the AISI 304 sheet was obtained from the tensile test, and its material model could be represented by a power-law according to equation (1). The blank holder and die were set as a 2D solid surface (rigid bodies). The blank holder-sheet interface was segmented into six areas, as shown in Figure 4. Note that only half

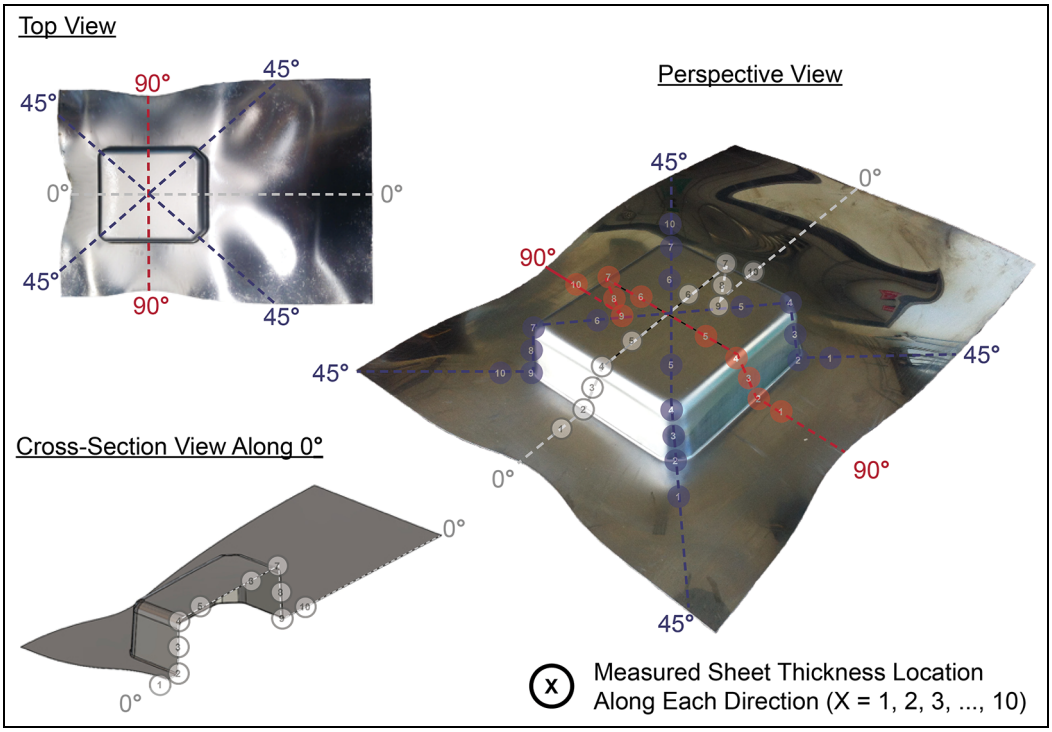

Figure 3. Sheet thickness measurement locations.

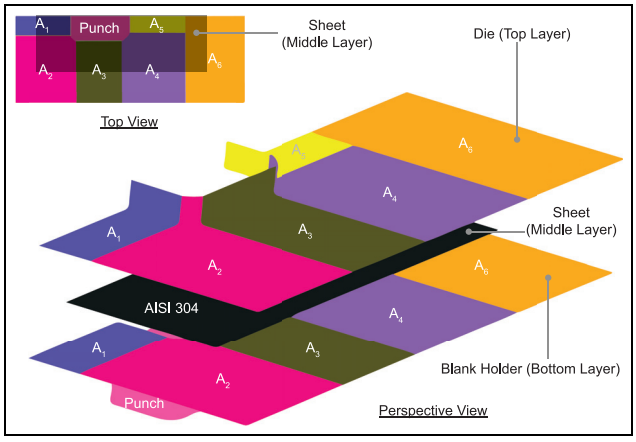

Figure 4. Segmented areas in the FEA model.

of the deep-drawing setup was modeled due to its symmetry. The blank sheet was modeled as deformable bodies. The sheet had 9971 elements of eight nodes, solid shell, brick topology element with an initial thickness of 0.4 mm.

The initial COF values of all the segmented blank-sheet areas were set to be 0.125, according to the strip-drawing test. The selected friction model for the FEA setup was Coulomb Arctangent (Velocity). During the FEA simulation, the punch was set to be stationary at the bottom, while the die was moved downward until it reached the depth of 30 mm. The clamping force from each gas spring was transmitted to the blank holder plate, which was modeled as a deformable body. The overall numerical methods used in this study are shown in Figure 5. The FEA setup was verified by comparing the sheet thickness values at different locations with those of the experiments. If the FEA results had errors within 15%, there were considered acceptable. Then, the same FEA model was used to vary localized friction or VCOF through the Design of Experiment (DOE). Within the DOE, the best (fittest) regression model was evaluated. The prepared regression model was then used to predict sheet thinning under different VCOF values.

Table 2 shows the DOE of the considered VCOF values in the segmented blank-sheet interfaces. The range of VCOF values was from 0.050 to 0.425 (77 cases) and set in the FEA model. The minimum VCOF value (0.050) was based on the study of Bernoulli et al.,[30] and the maximum VCOF value (0.425) was obtained from the report of Buckley.[31] The set VCOF values were used as the input parameters, and the sheet thickness values obtained from the FEA results were then used as the response parameters in the

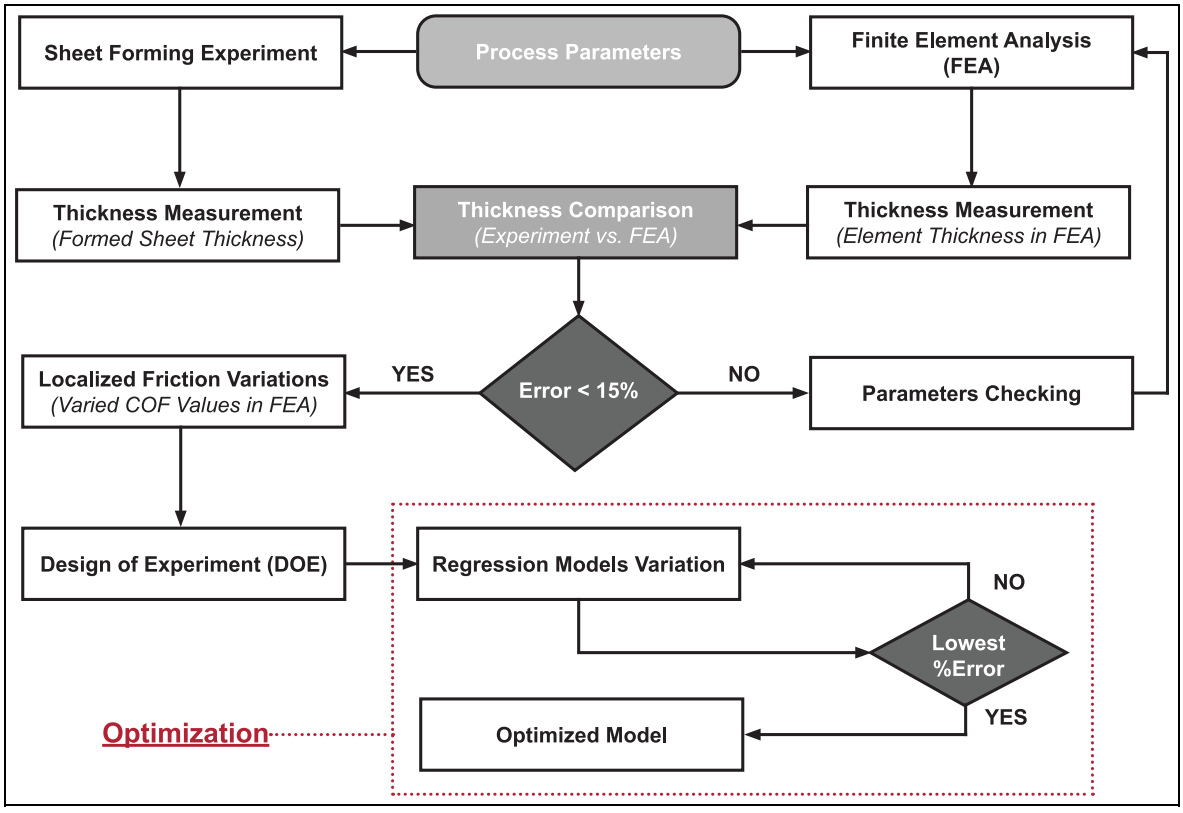

Figure 5. Flow chart of the methods used in this study to investigate the effects of VCOF to sheet thinning in deep-drawing.

Table 2. DOE of the considered VCOF values in the segmented blank-sheet interfaces.

FEA cases	Variable coefficient of friction (VCOF)					
	A_1	A_2	A_3	A_4	A_5	A_6
1	0.175	0.175	0.175	0.425	0.175	0.175
2	0.300	0.050	0.050	0.300	0.300	0.300
3	0.175	0.175	0.175	0.175	0.175	0.175
4	0.050	0.300	0.050	0.300	0.300	0.050
5	0.050	0.300	0.050	0.050	0.300	0.050
6	0.050	0.050	0.050	0.050	0.050	0.050
7	0.050	0.050	0.050	0.050	0.300	0.300
8	0.300	0.300	0.300	0.300	0.300	0.050
9	0.300	0.300	0.050	0.300	0.300	0.050
10	0.300	0.050	0.300	0.050	0.050	0.050
11	0.300	0.300	0.050	0.050	0.300	0.300
12	0.300	0.050	0.300	0.300	0.050	0.300
13	0.175	0.175	0.175	0.175	0.050	0.175
14	0.300	0.300	0.300	0.050	0.050	0.300
15	0.300	0.300	0.050	0.300	0.050	0.050
16	0.300	0.300	0.050	0.300	0.050	0.300
17	0.300	0.300	0.050	0.050	0.300	0.050
18	0.300	0.300	0.300	0.300	0.300	0.300
19	0.050	0.300	0.300	0.050	0.300	0.300
20	0.050	0.300	0.050	0.300	0.050	0.300
21	0.050	0.300	0.050	0.050	0.050	0.050
22	0.300	0.300	0.300	0.050	0.050	0.050
23	0.050	0.300	0.300	0.050	0.050	0.300
24	0.175	0.175	0.175	0.050	0.175	0.175
25	0.050	0.050	0.050	0.300	0.300	0.050
26	0.175	0.175	0.425	0.175	0.175	0.175
27	0.050	0.300	0.300	0.300	0.300	0.300
28	0.050	0.050	0.300	0.300	0.050	0.300
29	0.300	0.300	0.300	0.050	0.300	0.300
30	0.300	0.300	0.300	0.050	0.300	0.050
31	0.050	0.300	0.050	0.050	0.300	0.300
32	0.300	0.300	0.050	0.050	0.050	0.300
33	0.300	0.300	0.050	0.300	0.300	0.300
34	0.050	0.050	0.300	0.050	0.300	0.050
35	0.050	0.050	0.300	0.300	0.300	0.050
36	0.300	0.300	0.300	0.300	0.050	0.300
37	0.050	0.050	0.050	0.300	0.300	0.300
38	0.175	0.175	0.175	0.175	0.425	0.175
39	0.050	0.050	0.050	0.300	0.050	0.050
40	0.175	0.175	0.175	0.175	0.175	0.050
41	0.050	0.050	0.300	0.300	0.300	0.300
42	0.175	0.425	0.175	0.175	0.175	0.175
43	0.050	0.300	0.300	0.300	0.050	0.050
44	0.175	0.175	0.175	0.175	0.175	0.425
45	0.300	0.050	0.050	0.050	0.050	0.050
46	0.175	0.175	0.050	0.175	0.175	0.175
47	0.300	0.300	0.050	0.050	0.050	0.050
48	0.300	0.050	0.050	0.050	0.300	0.050
49	0.300	0.050	0.050	0.050	0.300	0.300
50	0.050	0.300	0.300	0.300	0.050	0.300
51	0.050	0.300	0.050	0.300	0.050	0.050
52	0.050	0.175	0.175	0.175	0.175	0.175
53	0.050	0.050	0.300	0.050	0.050	0.300
54	0.050	0.300	0.050	0.300	0.300	0.300
55	0.300	0.050	0.300	0.050	0.300	0.300
56	0.300	0.050	0.300	0.300	0.050	0.050
57	0.050	0.300	0.050	0.050	0.050	0.300
58	0.050	0.050	0.050	0.050	0.050	0.300
59	0.425	0.175	0.175	0.175	0.175	0.175

(continued)

Table 2. Continued

FEA cases	Variable coefficient of friction (VCOF)					
	A_1	A_2	A_3	A_4	A_5	A_6
60	0.050	0.050	0.300	0.050	0.300	0.300
61	0.050	0.050	0.050	0.050	0.300	0.050
62	0.050	0.050	0.300	0.300	0.050	0.050
63	0.300	0.050	0.300	0.050	0.050	0.300
64	0.050	0.300	0.300	0.050	0.050	0.050
65	0.175	0.050	0.175	0.175	0.175	0.175
66	0.300	0.050	0.050	0.300	0.050	0.300
67	0.300	0.050	0.300	0.050	0.300	0.050
68	0.300	0.050	0.300	0.300	0.300	0.300
69	0.300	0.300	0.300	0.300	0.050	0.050
70	0.300	0.050	0.300	0.300	0.300	0.050
71	0.300	0.050	0.050	0.050	0.050	0.300
72	0.050	0.050	0.300	0.050	0.050	0.050
73	0.050	0.300	0.300	0.050	0.300	0.050
74	0.050	0.050	0.050	0.300	0.050	0.300
75	0.300	0.050	0.050	0.300	0.050	0.050
76	0.300	0.050	0.050	0.300	0.300	0.050
77	0.050	0.300	0.300	0.300	0.300	0.050

optimization model. Note that the response values were not shown in Table 2.

Three regression models were selected to determine the best (fittest) model.[32] The first model was the Linear Regression, which could be written, as shown in equation (3):

$$r = \beta_0 + \beta_1 \cdot x + \beta_2 \cdot y \tag{3}$$

where r is the responding factor, x and y are the input factors, βi is the coefficient of the fit-model term, and i is the number of fit-model terms. The second regression model was the Response Surface Method (RSM), as shown in equation (4).

$$y = \beta_0 + \beta_1 \cdot x + \beta_2 \cdot y + \beta_3 \cdot x^2 + \beta_4 \cdot y^2 + \beta_5 \cdot x \cdot y \tag{4}$$

The last regression model was the Polynomial Regression, as written in equation (5).

$$\begin{aligned} y = {} & \beta_0 + \beta_1 \cdot x + \beta_2 \cdot y + \beta_3 \cdot x^2 + \beta_4 \cdot y^2 \\ & + \beta_5 \cdot x^3 + \beta_6 \cdot y^3 + \beta_7 \cdot x \cdot y^2 + \beta_8 \cdot y \cdot x^2 + \beta_9 \cdot x \cdot y \end{aligned} \tag{5}$$

The input values (VCOF) from Table 2 and the response values (sheet thickness values) obtained from the FEA results were used to calculate the βi values of all three regression models. Then, the accuracy of these models was determined by using the additional FEA conditions shown in Table 3.

The optimization method of the coefficients of each regression method was determined by using MATLAB. The predicted sheet thickness values of each regression model were compared with those of the FEA results. The prediction error ($\%Error$) values were calculated by using equation (6).

$$\%Error = abs|t_r - t_{FEA}| \times 100/t_{FEA} \tag{6}$$

where t_r is the predicted sheet thickness value, and t_{FEA} is the sheet thickness value from the FEA results. Note that the $\%Error$ values were calculated at the three measurement directions (0°, 45°, and 90°) and ten measurement points, as displayed in Figure 3. Afterward, the significant analysis of the βi values in the best (fittest) regression model was carried out to observe the influences of VCOF on the sheet thinning values.

In summary, the response surface method from the DOF having two-level full factorial analysis with six continuous factors was used extract the thinning value at each simulation.

Results and discussions

FEA model verification

An example sheet thickness results comparison between those of experiment and FEA is shown in Figure 6.

It could be clearly observed that the results of both the experiment and FEA were in agreement according to the calculated percentage of thinning values. Note that the locations number eight were prone to thinning because the nearby areas (locations number seven and locations number nine) were the cup corners, restricting the material flow and causing the sheet to elongate with reduced thickness. Location numbers 1 and 10 provided the lowest percentage of thinning values because these areas were tightly compressed between the die and blank holder, prohibiting the sheet from moving and deforming. According to the FEA results, the error between FEA and experimental results was below 15%, which was considered acceptable for this study.

Table 3. Additional FEA conditions with different VCOF values to evaluate the accuracy of the three regression models.

Additional FEA cases	Variable coefficient of friction (VCOF)					
	A_1	A_2	A_3	A_4	A_5	A_6
Add1	0.150	0.120	0.220	0.180	0.080	0.080
Add2	0.080	0.080	0.080	0.080	0.080	0.080
Add3	0.220	0.220	0.220	0.220	0.220	0.220
Add4	0.080	0.080	0.180	0.220	0.120	0.150
Add5	0.280	0.160	0.060	0.090	0.100	0.230

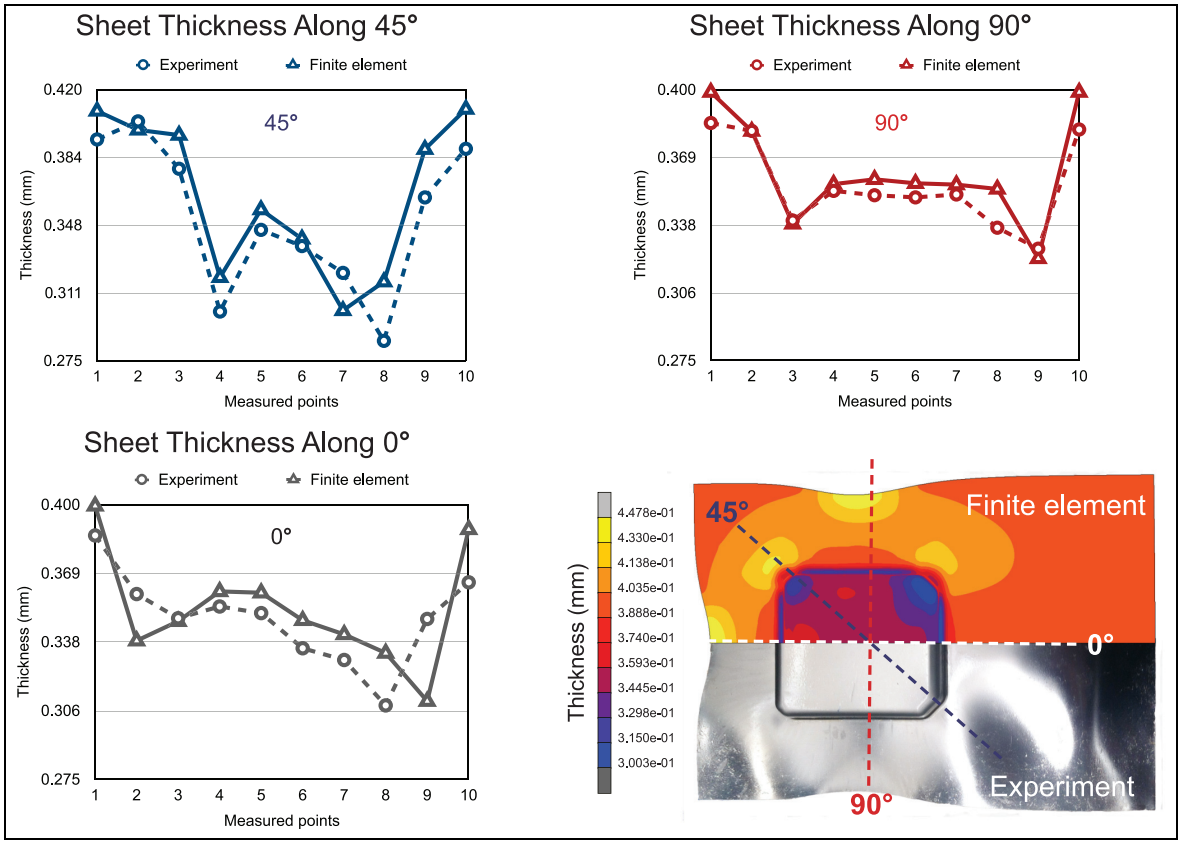

Figure 6. Comparison of the sheet thinning values between the FEA and experimental results (VCOF = 0.125 for all blank-sheet interfaces).

Results of the investigated regression models

The three regression models were developed by using the data from Table 2 to determine their βi values, and the additional conditions shown in Table 3 were used to determine the *%Error* values. Table 4 shows the *%Error* values of the investigated regression models.

The results showed that the Linear Regression model provided the best fitting model to predict the sheet thickness values (1.28% Average, and 6.73% Maximum). The RSM model provided the higher *%Error* values of (2.97% Average, and 7.84% Maximum). The Polynomial Regression model provided the highest *%Error* values (3.39% Average, and 21.89% Maximum). The results demonstrated that the increasing high order fitting term led to increasing *%Error* values. As a result, sheet thinning could simply be modeled by the Linear Regression model. In other words, the sheet thinning value had a linear relationship with the VCOF values.

The following equation showed the linear regression model obtained from this study.

$$t_n = C + \beta_0 \cdot f_1 + \beta_1 \cdot f_2 + \beta_2 \cdot f_3 + \beta_3 \cdot f_4 + \beta_4 \cdot f_5 + \beta_5 \cdot f_6 \quad (7)$$

where t_n is the predicted sheet thickness at a measured location, n is the measured location, f_1–f_6 are VCOF

Table 4. The *%Error* values of the investigated regression models.

Fitting models	Additional FEA cases	0°-Direction (*%Error*)		45°-Direction (*%Error*)		90°-Direction (*%Error*)	
		Max. (%)	Avg. (%)	Max. (%)	Avg. (%)	Max. (%)	Avg. (%)
Liner regression	Add1	1.82	0.85	4.85	1.61	3.37	0.98
	Add2	3.40	0.94	4.47	1.03	1.87	0.45
	Add3	2.52	1.32	5.14	2.13**	3.13	1.29
	Add4	2.20	1.10	5.72	1.69	6.73*	1.57
	Add5	2.77	1.31	3.94	1.64	2.25	1.24
Response surface method (RSM)	Add1	4.29	1.92	7.84*	2.97**	5.67	2.92
	Add2	2.27	0.64	5.31	0.86	2.52	0.44
	Add3	2.99	1.24	5.98	2.51	6.13	1.58
	Add4	2.80	1.23	7.75	2.19	4.53	1.35
	Add5	3.05	1.55	5.53	2.02	2.77	1.54
Polynomial regression	Add1	6.91	2.27	12.02	3.31	5.64	2.47
	Add2	5.69	2.47	12.10	3.46	5.30	2.63
	Add3	10.02	4.01	17.46	6.67**	15.90	4.60
	Add4	7.44	2.05	9.28	3.01	15.23	2.68
	Add5	13.01	2.76	21.89*	4.58	14.04	2.81

*Represents the highest *%Error* value of each fitting model, and **represents the highest average *%Error* value of each fitting model.

values of the segmented areas (A_1–A_6), C and βi are the constants. The predictions by using the Linear Regression model were also mapped with the results of the deep-drawing experiment, as illustrated in Figure 7. The deep-drawing experiment result showed that tearing occurred in the bottom corners of the part. The two locations shown in the figure were locations four and seven, respectively, of the 45°-direction. The Linear Regression models of locations four and seven are shown in equations (8) and (9), respectively.

$$t_4 = 0.282 - 0.0112 \cdot f_1 - 0.023 \cdot f_2 - 0.055 \cdot f_3 - 0.097 \cdot f_4 - 0.002 \cdot f_5 - 0.0044 \cdot f_6 \quad (8)$$

$$t_7 = 0.2784 - 0.0049 \cdot f_1 - 0.001 \cdot f_2 - 0.0292 \cdot f_3 - 0.0274 \cdot f_4 - 0.0023 \cdot f_5 - 0.0024 \cdot f_6 \quad (9)$$

where t_4 is the predicted sheet thickness at location four, and t_7 is the predicted sheet thickness at location seven. The sheet thinning behaviors were affected by the different contributions of the VCOF values in different areas. Some segmented areas having higher coefficients would influence more than the others did. For instance, areas A_3 and A_4 had higher coefficients in both locations. Thus, friction reductions should be focused at these locations.

The significant factor analysis of the Linear Regression model was carried out by using the two-sample test (t-test) method.[32] Since the output response with 95% ($\alpha = 0.05$) confidence level was set, and the experiment degree of freedom (DOF) was $2n - 2 = 152$, the significant t-value, t, of variable factor equal to 1.645. If a t-value of the observed term was large enough ($|t| \geqslant 1.645$), it was concluded that the observed term was significant. The significant factor analysis results of the Linear Regression model are shown in Table 5. Nodes 1–10 represented the measuring locations in Figure 3.

The values of nodes two and nine (die radii) were note shown here because the significant variable values were lower than 1.645. The results obtained from Table 5 show how sheet thinning at different locations were affected by the contributions of different VCOF in different areas. The results showed that sheet thinning at any location was affected by the contributions of at least two segmented areas. However, sheet thinning was not affected by all of the considered areas. As a result, localized and variable frictions affect the formability in deep-drawing. Based on the results, the VCOF values in different areas could be controlled (optimized) to prevent tearing at different locations. Ultimately, the more precise or complex shape parts in deep-drawing could be obtained by localized friction control.

Conclusion

This study experimentally and numerically investigated the effect of the localized friction on the sheet thinning of AISI 304 in the deep-drawing process. Six segmented areas of the blank-sheet interfaces were investigated by varying the coefficient of friction values from 0.050 to 0.425. The integration of the Finite Element Analysis (FEA) and the regression analysis was used to predict sheet thinning along the 0°, 45°, and 90° directions. Three regression models (Linear Regression, Response Surface Model (RSM), and Polynomial Regression) were evaluated. The results showed that the Linear regression model was the best (fittest) model to predict sheet thinning affected by localized friction. The significant factor analysis of the Linear Regression model was carried out. The results showed that sheet thinning at

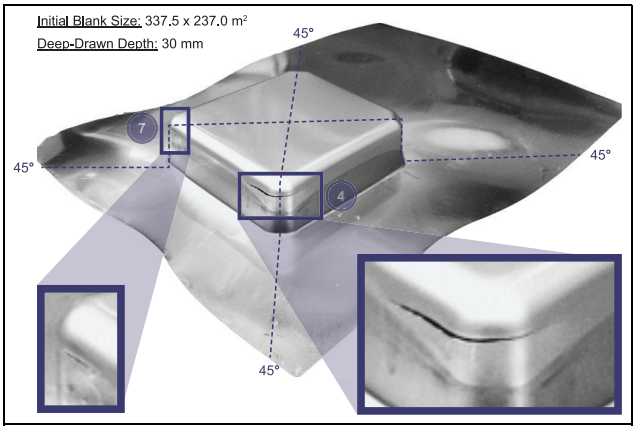

Figure 7. The tearing locations in the deep-drawing experiment and linear regression model predictions.

any location was affected by the contributions of at least two segmented areas. The variable coefficient of friction (VCOF) values in different areas could be controlled (optimized) to prevent tearing at different locations.

Declaration of conflicting interests

The author(s) declared no potential conflicts of interest with respect to the research, authorship, and/or publication of this article.

Funding

The author(s) disclosed receipt of the following financial support for the research, authorship, and/or publication of this article: This study was supported by the NSTDA University-Industry Research Collaboration (NUI-RC) [grant number NUI-RC-M33-12-56-002D], LPN Metallurgical Research Center Co., Ltd., Diamond Brand Co., Ltd., National Metal and Materials Technology Center (MTEC), and Department of Mechanical Engineering, Faculty of Engineering, Khon Kaen University.

ORCID iD

Numpon Mahayotsanun https://orcid.org/0000-0002-3703-1180

References

1. Endelt B, Tommerup S and Danckert J. A novel feedback control system – Controlling the material flow in deep drawing using distributed blank-holder force. *J Mater Process Technol* 2013; 213(1): 36–50.
2. Polyblank JA, Allwood JM and Duncan SR. Closed-loop control of product properties in metal forming: A review and prospectus. *J Mater Process Technol* 2014; 214(11): 2333–2348.
3. Kitayama S, Hamano S and Yamazaki K. Development of a simple closed-loop type algorithm for determination of variable blank holder force trajectory and its

Table 5. Significant factor analysis results of the linear regression model.

Direction	Significant analysis	Node 1	Node 3	Node 4	Node 5	Node 6	Node 7	Node 8	Node 10
0°-Direction	Significant	A_2^*, A_4	A_1^*, A_2, A_3^*	A_1^*, A_3^*, A_4	A_1^*, A_3^*, A_4^*	A_3^*, A_4^*	A_3^*, A_4^*	A_2^*, A_3^*, A_4^*, A_5^*	A_3^*, A_4^*, A_5^*
	Coefficient	−0.0086*	−0.0217*	−0.0220*	−0.0167*	−0.0336*	−0.0250*	−0.0071*	−0.0086*
		−0.0044	−0.0065	−0.0185*	−0.0304*	−0.0192*	−0.0205*	−0.0134*	−0.0085*
			−0.0174*	−0.0117	−0.0145*			−0.0090*	+ 0.0085*
								−0.0088*	
45°-Direction	Significant	A_1^*, A_2^*, A_3^*, A_4^*	A_2^*	A_2^*	A_1^*, A_3^*, A_4^*	A_3^*, A_4^*	A_3^*, A_4^*	A_3, A_4^*	A_1^*, A_2^*, A_3^*, A_4^*
	Coefficient	−0.0065*	−0.0316*	−0.0230*	−0.0158*	−0.0378*	−0.0292*	−0.0235	−0.0064*
		+ 0.0030*			−0.0341*	−0.0200*	−0.0274*	−0.0371*	+ 0.0030*
		−0.0123*			−0.0154*				−0.0124*
		+ 0.0021*							+ 0.0022*
90°-Direction	Significant	A_4^*	A_1, A_3^*	A_1, A_3^*, A_4^*	A_1, A_3^*, A_4^*	A_1, A_3^*, A_4^*	A_1, A_3^*, A_4^*	A_1, A_3^*	A_4^*
	Coefficient	−0.0050*	−0.0061	−0.0084,	−0.0094	−0.0094	−0.0084	−0.0061	−0.0050*
			−0.0401*	−0.0506*	−0.0398*	−0.0398*	−0.0506*	−0.0401*	
				−0.0114*	−0.0141*	−0.0141*	−0.0114*		

*High-significant factor ($|t\text{-value}| > 2.326$, $\alpha < 0.01$ or Confident level > 99%).

applications to square cup deep drawing. *Adv Mech Eng* 2010; 2: 497350.
4. Allwood JM, Duncan SR, Cao J, et al. Closed-loop control of product properties in metal forming. *CIRP Ann* 2016; 65(2): 573–596.
5. Padmanabhan R, Oliveira MC, Alves JL, et al. Influence of process parameters on the deep drawing of stainless steel. *Finite Elem Anal Des* 2007; 43(14): 1062–1067.
6. Su S, Jiang Y and Xiong Y. Multi-point forming springback compensation control of two-dimensional hull plate. *Adv Mech Eng* 2020; 12(4): 1687814020916094.
7. du Toit M and Steyn HG. Comparing the formability of AISI 304 and AISI 202 stainless steels. *J Mater Eng Perform* 2012; 21(7):1491–1495.
8. Kim J, Noh H-G, Song W-J, et al. Comparative numerical analysis of sheet formed into a V-shaped die using conventional and electromagnetic forming processes. *Adv Mech Eng* 2014; 6: 240789.
9. Ko D-C, Ko D-H, Kim J-H, et al. Development of a partition panel of an Al6061 sheet metal part for the improvement of formability and mechanical properties by hot forming quenching. *Adv Mech Eng* 2017; 9(2): 1687814017691213.
10. Oh KS, Oh KH, Jang JH, Kim DJ, et al. Design and analysis of new test method for evaluation of sheet metal formability. *J Mater Process Technol* 2011; 211(4): 695–707.
11. Sniekers RJJM. *Friction in deep drawing*. Eindhoven: Technische Universiteit Eindhoven, 1996.
12. Aleksandrović S, Stefanović M and Taranović D. Variable blank holding force as a factor of tribological influence on deep drawing. *Tribol Ind* 2000; 22: 5–9.
13. Hassan MA, Takakura N and Yamaguchi K. A novel technique of friction aided deep drawing using a blankholder divided into four segments. *J Mater Process Technol* 2003; 139(1): 408–413.
14. Olguner S and Bozdana AT. The effect of friction coefficient on punch load and thickness reduction in deep drawing process. *Int J Mater Res* 2016; 3: 64–68.
15. Gil I, Mendiguren J, Galdos L, et al. Influence of the pressure dependent coefficient of friction on deep drawing springback predictions. *Tribol Int* 2016; 103: 266–273.
16. Tekaut İ. The effects of friction coefficient on formability behaviour of dual phase steel. *Mater Res* 2019; 22(5): 1–6.
17. Trzepiecinski T. A study of the coefficient of friction in steel sheets forming. *Metals* 2019; 9(9): 988.
18. Quesada A, Gauchia A, Álvarez-Caldas C, et al. Material characterization for FEM simulation of sheet metal stamping processes. *Adv Mech Eng* 2014; 6: 167147.
19. Mac T-B, Do V-C and Nguyen D-T. A study of combined finite element method simulation/experiment to predict forming limit curves of steel DP350 sheets. *Adv Mech Eng* 2018; 10(4): 1687814018768148.
20. Chen D-C, Cheng-Yu L and Lai Y-Y. Finite element analysis of deep drawing. *Adv Mech Eng* 2019; 11(9): 1687814019874561.
21. Chen L, Bai Y, Jiang Z, et al. Numerical and experimental studies on wrinkling control methods of sheet metal part with high curvature and large flange in rubber forming. *Adv Mech Eng* 2019; 11(10): 1687814019883787.
22. Wang Y, Liu D-Z and Li R. Numerical investigation for the flexible stretch-stamp forming process of sheet metal. *Adv Mech Eng* 2019; 11(1): 1687814018819287.
23. The-Thanh L, Tien-Long B, The-Van T, et al. A study on a deep-drawing process with two shaping states for a fuel-filter cup using combined simulation and experiment. *Adv Mech Eng* 2019; 11(8): 1687814019872674.
24. Yao Z, Li Y, Yang M, et al. Parameter optimization for deformation energy and forming quality in single point incremental forming process using response surface methodology. *Adv Mech Eng* 2017; 9(7): 1687814017710118.
25. Hong J-J and Yeh W-C. Application of response surface methodology to establish friction model of upset forging. *Adv Mech Eng* 2018; 10(3): 1687814018766744.
26. Abdelrahim H, Mohamed HB, La P, et al. Effect of multiple warm rolling on microstructure and mechanical properties of 304 stainless steel prepared by aluminothermic reaction. *Adv Mech Eng* 2020; 12(5): 1687814019850998.
27. Meng Y, Zhang J-Y, Zhan H, et al. Effects of subsequent treatments on the microstructure and mechanical properties of SKD11 tool steel samples processed by multi-stage thixoforging. *Mater Sci Eng A* 2019; 762: 138070.
28. Koowattanasuchat P, Mahayotsanun N, Mahabunphachai S, et al. Influences of contact pressure, sliding velocity, lubricant, bending angle and surface texture on friction in stainless steel strip drawing. *Adv Mater Process Technol* 2015; 1: 3–4.
29. Koowattanasuchat P, Sucharitpwatskul S, Mahabunphachai S, et al. Effect of bending angles to friction in strip drawing of stainless steel. In: *7th international conference on tribology in manufacturing processes*, Phuket, Thailand, 28 February 2016, pp. 165–170.
30. Bernoulli D, Cao SC, Lu J, et al. Enhanced repeated frictional sliding properties in 304 stainless steel with a gradient nanostructured surface. *Surf Coat Technol* 2018; 339: 14–19.
31. Buckley DH. Friction behavior of 304 stainless steel of varying hardness lubricated with benzene and some benzyl structures. *National Aeronautics and Space Administration*, 1974. Contract No.: NASA TN D-7787.
32. Montgomery DC. *Design and analysis of experiments*. 8th ed. New York: Wiley & Sons Inc., 2013, pp. 27–40.